Environ Geol (2007) 52:269–281
DOI 10.1007/s00254-006-0476-x

ORIGINAL ARTICLE

The role of saline solution properties on porous limestone salt weathering by magnesium and sodium sulfates

E. Ruiz-Agudo · F. Mees · P. Jacobs · C. Rodriguez-Navarro

Received: 16 June 2006 / Accepted: 16 August 2006 / Published online: 13 September 2006

Abstract Saline solution properties, viscosity in particular, are shown to be critical in salt weathering associated with sodium and magnesium sulfate crystallization in porous limestone. The crystallization of sodium and magnesium sulfate within a porous limestone has been studied at a macro- and microscale using different techniques, including mercury intrusion porosimetry, environmental scanning microscopy and X-ray computed tomography. Such analysis enabled the visualization of the crystallization process in situ, and at high magnification, yielding critical information as to where and how salts crystallize. Sodium sulfate decahydrate (mirabilite) tends to crystallize in large pores as euhedral micron-sized crystals formed at low supersaturation near to the surface of the stone. In contrast, magnesium sulfate heptahydrate (epsomite) tends to precipitate as anhedral wax-like aggregates formed at high supersaturation and distributed homogeneously throughout the stone pore system filling large and small pores. While the former crystallization behavior resulted in scale formation, the latter led to crack development throughout the bulk stone. Ultimately, the contrasting weathering behavior of the two sulfates is explained by considering differences in flow dynamics of solutions within porous materials that are mainly connected with the higher viscosity of magnesium sulfate saturated solution (7.27 cP) when compared with sodium sulfate saturated solution (1.83 cP). On the basis of such results, new ways to tackle salt weathering, particularly in the field of cultural heritage conservation, are discussed.

Keywords Stone decay · Sodium sulfate · Magnesium sulfate · Salt weathering · ESEM

E. Ruiz-Agudo · C. Rodriguez-Navarro (✉)
Departamento de Mineralogía y Petrología,
Universidad de Granada, Fuentenueva s/n,
18002 Granada, Spain
e-mail: carlosrn@ugr.es

F. Mees · P. Jacobs
Department of Geology and Soil Science,
Ghent University, Krijgslaan 281 S8,
9000 Ghent, Belgium

Introduction

The crystallization of soluble salts in porous materials is one of the major causes of rock decay in nature (Evans 1970; Winkler and Singer 1972), and weathering of stone buildings and other engineering structures (Winkler 1994; Goudie and Viles 1997; Rodriguez-Navarro and Doehne 1999a). Salt weathering appears to be an ubiquitous phenomenon, affecting many rock types and man-made materials (e.g., bricks, mortars and concrete) all around the world: from cold deserts in Antarctica, to hot deserts in Africa, to coastal areas, to urban environments (Evans 1970; Goudie and Viles 1997; Rodriguez-Navarro and Doehne 1999a). Moreover, salt weathering has been suggested to be an universal phenomenon, contributing to the modeling of some aspect of Martian landscapes and rocks (Malin 1974; Rodriguez-Navarro 1998).

When water accesses the pore network of a stone, it may carry various salts in solution. Several mechanisms can subsequently cause crystal growth. For example, cooling during nighttime can cause crystallization of salts whose solubility increases with temperature (Thaulow and Sahu 2004). Most commonly, evaporation

may induce salt crystallization (Coussy 2006). When this happens, highly concentrated saline solutions may yield large volume of precipitates (Goudie and Viles 1997). A number of mechanisms have been proposed to explain the damage caused by soluble salts to porous materials. Proposed salt damage mechanisms include generation of crystallization pressure, hydration pressure, thermal expansion, osmotic pressure and chemical weathering (Rodriguez-Navarro and Doehne 1999a). Besides hydration pressure, which appears to be a non-existing phenomenon (it just seems to be crystallization pressure due to formation of an hydrated phase following dissolution of an anhydrous one: Rodriguez-Navarro et al. 2000a; Flatt 2002; Thaulow and Sahu 2004), all other mechanisms may to some degree contribute to the overall damage process. However, crystallization pressure appears to be the most relevant (Rodriguez-Navarro et al. 2000a; Scherer 1999, 2004; Flatt 2002; Steiger 2005a, b; Coussy 2006). The growth of a crystal in a confined space (pore) can exert a pressure sufficient to exceed the rupture modulus of most ornamental materials, including natural stone, mortars and bricks, causing their breakage (Winkler and Singer 1972; La Iglesia et al. 1997). It is generally accepted that the damage to porous stones arises from repeated cycles of crystallization/dissolution of soluble salts within the porous matrix of the stone (Coussy 2006). These processes can alter both the porosity and the pore size distribution of the stones, changing also their mechanical properties (compression strength, sclerometric resistance, microhardness) (Dei et al. 1999).

Although salts (i.e., sodium sulfate) were used early in the nineteenth century to test stone soundness towards freezing water (de Thury 1828), experimental evidence that growing crystals can exert pressure was first provided 150 years ago (Steiger 2005a). Using NMR, Rijniers et al. (2005) recently proved that salts can exert pressure inside pores. Since the early reports on the pressure generated by growing crystals, several authors have proposed models and equations that allow the evaluation of the crystallization pressure exerted by a crystal when it grows in a pore (e.g., Benavente et al. 1999; Scherer 1999; Steiger 2005a, b; Coussy 2006). Two different approaches have been traditionally considered. First, Correns (1949) related crystallization pressure to the degree of supersaturation in a solution. Weyl (1959) developed a general model for salt damage, considering Correns' equation as a special case. Weyl proposed that growth at a stressed crystal face requires the presence of a supersaturated solution film between the crystal face and its constraint. The so-called force of crystallization is a consequence of the deposition of matter on the growing crystal surface, at the crystal–pore wall interface. Subsequent modifications of Correns equation were developed, for instance by Xie and Beaudoin (1992), Benavente et al. (1999) and Scherer (1999). On the other hand, Everett (1961) related the crystallization pressure to the properties of curved interfaces between the crystal and the solution. Wellman and Wilson (1965), following Everett's work, developed a thermodynamic model for calculating the crystallization pressure of a salt, according to which salt crystallization would take place initially in larger pores with solution being supplied from the smaller capillaries. Recently, Scherer (2004), Steiger (2005a, b) and Coussy (2006) independently derived equations for the calculation of crystallization pressure considering both the degree of supersaturation of the solution and the effect of the curvature of the crystal–liquid interface. Furthermore, Coussy (2006) quantitatively addressed the important case of drying-induced salt crystallization in porous stones. Despite these efforts, the processes and pathways of salt damage are still poorly understood. Indeed, these seemingly well-accepted salt damage models do not explain many observed phenomena. For example, it has not been determined why some salts are more damaging than others. Calculations of salt crystallization pressure of many common salts (e.g., chlorides, sulfates and nitrates) (Winkler and Singer 1972) show that all of them could cause damage to even the strongest materials. In fact, the calculated crystallization pressure values were orders of magnitude higher than rupture modulus of most common building materials. However, there is overwhelming experimental evidence showing that, under equal experimental conditions (porous substratum, environmental conditions, initial salt concentration), some salts are extremely damaging (e.g. sodium sulfate and magnesium sulfate) while others are not (e.g., sodium chloride) (Goudie et al. 1997; Rodriguez-Navarro and Doehne 1999a). On the other hand, there is little agreement on the relative merits of each of the different parameters that contribute to or control salt weathering (stone properties, environmental conditions, and saline solution properties). The study of each parameter in isolation is a simplified way to obtain useful information concerning the knowledge of the key parameters controlling salt weathering.

Considering the importance of this decay mechanism, not only from a geomorphologic point of view, but also from a cultural and economic standpoint, it is essential to know the mechanisms of damage and the parameters controlling the process of salt weathering as a first step to design methods to mitigate this problem in

the fields of civil engineering and cultural heritage conservation. Here, differences in crystallization behavior and damage pattern of sodium and magnesium sulfates have been studied. These two salts are extensively found in both decayed cement structures and porous building stones (Goudie and Viles 1997; Rodriguez-Navarro and Doehne 1999a; Rodriguez-Navarro et al. 2000a). Both are highly damaging and show completely different crystallization pattern, as will be shown below; however, their damage mechanism has not yet been clarified. This study reveals some key parameters which control various aspects of salt damage of porous stone, such as where crystallization occurs and in what kind of pores. The results of this study may help elucidate why sodium and magnesium sulfates are so damaging and display such a contrasting weathering behavior, which is critical to designing possible solutions to reduce their damage.

Materials and methods

Studied salts

The Na_2SO_4–H_2O system includes two stable phases: thenardite (Na_2SO_4), the anhydrous phase that, in equilibrium, precipitates directly from solution at temperature (T) above 32.4°C, and mirabilite ($Na_2SO_4{\cdot}10H_2O$), the stable phase below this T. The solubility of thenardite and mirabilite decreases with increasing and decreasing T, respectively. Mirabilite dehydrates to thenardite at relative humidity (RH) below 71% (20°C). $Na_2SO_4{\cdot}10H_2O$ belongs to the monoclinic crystal system with space group $P2_1/c$. Mirabilite consists of chains of Na^+ ions coordinated by bridging water molecules, extending parallel to c-axis. Anions form linear chains. Adjacent SO_4^{2-} ions are bridged by two water molecules not involved in the cation chains (Levy and Lisensky 1978). Five polymorphs of anhydrous sodium sulfate (I, II, III, IV and V) have been identified (Naruse et al. 1987). Sodium sulfate heptahydrate ($Na_2SO_4{\cdot}7H_2O$) has been described as precipitating at T below the mirabilite/thenardite transition point. However, this phase is metastable and has not been clearly identified in nature.

On the other hand, the only naturally occurring members of the $MgSO_4{\cdot}nH_2O$ series on Earth are epsomite ($MgSO_4{\cdot}7H_2O$, 51 wt% water), hexahydrite ($MgSO_4{\cdot}6H_2O$, 47 wt% water) and kieserite ($MgSO_4{\cdot}H_2O$, 13 wt% water). In aqueous systems, epsomite is stable at T below 48.4°C, hexahydrite is stable in the T range 48.4–68°C, and kieserite is stable at $T > 68$°C (Robson 1927). All of these salts consist of SO_4 tetrahedra and $Mg(O,H_2O)_6$ octahedra; some include extra-polyhedral water (water that is not in octahedral coordination with Mg). Epsomite transforms readily to hexahydrite by loss of extra-polyhedral water; this transition is reversible and occurs at 50–55% RH at 298 K and at lower T as the activity of water diminishes (Vaniman et al. 2004). $MgSO_4{\cdot}7H_2O$ belongs to the orthorhombic crystal system with space group $P2_12_12_1$ (Ramalingom et al. 2003).

Occurrences of magnesium and sodium sulfate salts in nature are quite common and distributed worldwide (Braitsch 1971; Goudie and Cooke 1984). Examples of their decay effects on geologic settings and ornamental materials used in the built and sculptural heritage are numerous (see review by Goudie and Viles 1997). Both salts are commonly used in accelerated decay testing of stone because their crystallization is highly damaging (ASTM 1997; Rodriguez-Navarro and Doehne 1999a). In fact, both salts typically rank as the most effective salts in salt weathering experiments (Goudie 1986, 1993).

Stone characterization

The damaging effects of sodium and magnesium sulfates crystallization within a natural porous medium were studied using a porous biomicritic limestone (calcarenite). A porous limestone was selected as model material for salt crystallization tests because such stone type is commonly used in the sculptural and architectural heritage and is highly affected by salt weathering (Rodriguez-Navarro and Doehne 1999a). The calcarenite was quarried in the Santa Pudia area (15 km SW from Granada, Spain). It is buff colored, quite porous and easy to quarry and carve. These characteristics led to its extensive use in the Andalusian's architectural and sculptural heritage (Rodriguez-Navarro 1994).

Porosity and pore size distribution of the calcarenite were determined by mercury intrusion porosimetry (MIP, Micromeritics Autoscan 6500), using stone blocks (ca. 2 cm^3) that were dried overnight in an oven (110°C). The Washburn equation relates the applied pressure, P, to the radius, r, of cylindrical pores intruded with mercury: $P = -2\gamma \cos\theta/r$, where γ is the Hg surface tension (0.480 N/m), and θ is the Hg–solid contact angle. An advancing contact angle of 130° was selected as an average value for both stone (calcite) and salts because it is typical for most solids (Kaneuji et al. 1980; Good and Mikhail 1981; Lowell and Shields 1983; Katz and Thompson 1987). No attempt was made to measure Hg–stone and Hg–salt contact angles because the errors associated with such measurements

(Moscou and Lub 1981), plus the variations in contact angle associated with decreasing pore size and non-cylindrical pore geometry render such measurements useless in most cases (Good and Mikhail 1981).

Small oven-dried stone samples (~0.25 g) were used to obtain N_2 sorption isotherms at 77 K on a Micromeritics Tristar 3000 under continuous adsorption conditions. Prior to measurement, samples were heated at 200°C for 2 h and outgassed to 10^{-3} Torr using a Micromeritics Flowprep. BET analysis was used to determine the total specific surface area, while the BJH method was used to obtain pore size distribution curves (Gregg and Sing 1982).

Macroscale salt crystallization experiments

Saturated salt solutions were prepared from crystalline solid (Panreac, analytical grade) using deionized water, followed by filtering and heating to eliminate any undissolved salt crystals. Salt crystallization tests were carried out in a controlled environment (20 ± 2°C, and 45 ± 5% RH). The solutions were let to flow-through, evaporate and crystallize in the porous stone (see Rodriguez-Navarro et al. (2002) for details on the laboratory set-up). The solution evaporation rate was measured by continuous weighing of the stone–solution–beaker system. Salt crystals grown within the stone, as well as on its surface (efflorescence) were collected after crystallization experiments and examined by powder X-ray diffraction (XRD; Philips PW 1710 diffractometer) and environmental scanning microscopy (ESEM; Philips Quanta 400) with no prior treatment (i.e., no grinding) in order to infer their growth morphology.

Stone samples were collected after salt crystallization tests and dried overnight in an oven (110°C) prior to MIP analysis. Small stone pieces with sulfate subflorescence were collected from the stone slabs submitted to salt crystallization test and analyzed on an ESEM. Sulfate crystals distribution within the stone pore system was inferred by means of MIP analysis. Note that a small change in Hg contact angle should occur once the salts fill the limestone pores. However, the effects of such a change on MIP porosity and pore size distribution results are expected to be negligible.

Further analyses of salt distribution patterns within the stone pore system were done by means of polarized light microcopy and X-ray computed tomography (X-ray CT). X-ray CT is one of the few non-destructive techniques that are able to provide spatially resolved analytical information from the interior of opaque objects. For the petrographical study, thin sections were prepared after impregnation of the samples with a cold-setting polyester resin, avoiding contact with water at all stages. X-ray CT analyses were performed with a Skyscan 1072 scanner, which is a cone-beam system with a microfocus X-ray source. The scanner was operated using a 80 kV accelerating potential, a 0.45° rotation step between successive exposure positions, and averaging of four radiographs for each position. This technique allows the reconstruction of sets of parallel cross-sections, perpendicular to the axis of rotation within the scanner, which show distribution patterns of materials with different X-ray attenuation values, determined by density and chemical composition.

In situ ESEM microscale salt crystallization experiments

Since both Na- and Mg-sulfate can occur as hydrated phases, their study using conventional scanning electron microscope (SEM) is not feasible. In contrast, ESEM enables the observation of the different phases of hydrated salts at high magnification and without changing their hydration state, morphology and/or habit (Rodriguez-Navarro and Doehne 1999b). Furthermore, it allows high magnification, real-time observations of changes underwent upon crystallization and/or hydration/dehydration events. In other words, it enables the dynamic study of the crystallization process, a fact which has made this new technique relevant in building materials conservation, because it facilitates a correct analysis of the damage and weathering process caused by salts (Rodríguez-Navarro and Doehne 1999b). Thus, habit and size distribution of sulfate crystals, as well as microtextural and morphological modifications of the salts when they dissolve and recrystallize, were studied using an ESEM. Condensation and evaporation of water on salt samples were achieved by modifying T (Peltier stage) and gas pressure (water vapor) inside the ESEM chamber (6.5–3.5 Torr; 2–8°C; RH~32–94%), following the methodology outlined by Rodriguez-Navarro and Doehne (1999b). Time-lapse digital images were recorded on-line. Sodium and magnesium sulfate-laden limestone samples were submitted to condensation/evaporation cycles in the ESEM.

Results and discussion

Stone pore system and susceptibility to salt weathering

The stone selected for the study is well known to be susceptible to salt weathering (Rodriguez-Navarro

1994). The calcarenite overall porosity, determined by MIP, is 32.2%, with a mean pore radius of 13.5 μm. Calcarenite pore size distribution graphs (Fig. 1) show abundant macropores, with a maximum at ca. 30 μm. Smaller pores are also detected with secondary maximum at ca. 0.1 μm. The calcarenite shows a low specific surface area (0.815 m^2/g). The nitrogen absorption isotherm (Fig. 2a) is typical of non-microporous solids (Gregg and Sing 1982). The BJH plot (Fig. 2b) shows the presence of a significant amount of meso- and macropores (pore radius > 50 nm). Hydric properties are summarized in Table 1 (from Rodriguez-Navarro 1994).

Porosity and pore size distribution are key factors controlling the uptake and transport of fluids within a stone (Rodriguez-Navarro and Doehne 1999a). Stones such as the studied calcarenite with a high proportion of mesopores connected to large pores are very susceptible to salt weathering (Schaffer 1932; Benavente et al. 2004). The mesopores result in larger surface area for evaporation and slower solution transport, thus increasing the chances that high supersaturation ratios are reached below the stone surface resulting in detrimental subflorescence growth. In stones with larger pores, capillary rise is limited, surface area is lower, and solutions readily reach the stone surface where evaporation occurs, thus resulting in nearly harmless efflorescence growth (Rodriguez-Navarro et al. 2002). Hydric properties (Table 1) show that the calcarenite rapidly absorbs water, but dries slowly. Thus, salt solution will be taken up fast, but will remain within the stone pore system for enough time to precipitate as harmful subflorescence. Such behavior seems to contribute to the overall susceptibility of this stone towards salt weathering, as will be shown below.

Macroscale salt crystallization tests: sodium sulfate

Crystallization of Na-sulfate reduces the stone porosity (29.5%) and mean pore radius (3.1 μm). Deposition of Na-sulfate crystals takes place within the bigger pores of the stone (Fig. 1a), close to the surface, forming thin (few millimeters) stone surface layers that lift up successively (Fig. 3a, b). Salts tend to fall along with surface layer as damage progresses, as has been also shown by Rodriguez-Navarro and Doehne (1999a). This explains why the porosity is only reduced by a few percent (i.e., little salt remains in the pores of the

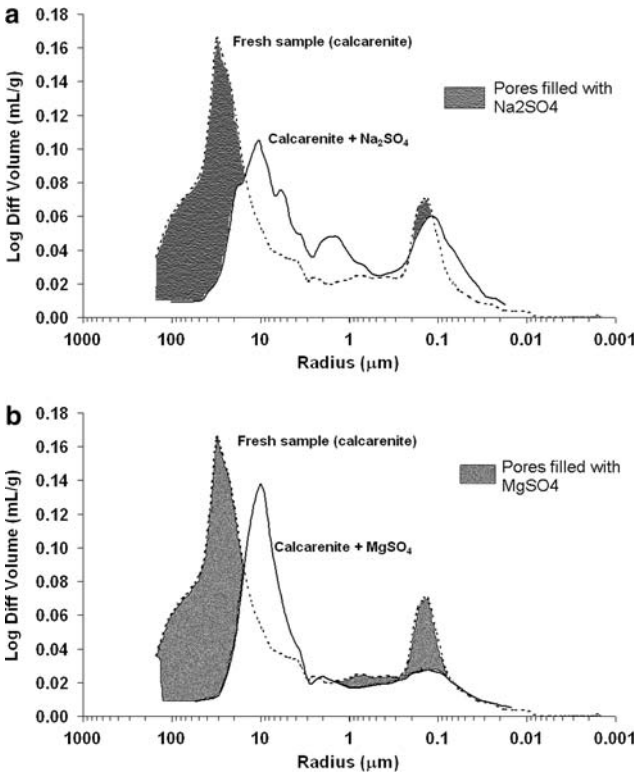

Fig. 1 Mercury intrusion porosimetry plots before and after salt crystallization in limestone pores: **a** sodium sulfate and **b** magnesium sulfate. *Shadowed areas* show pores filled with salts

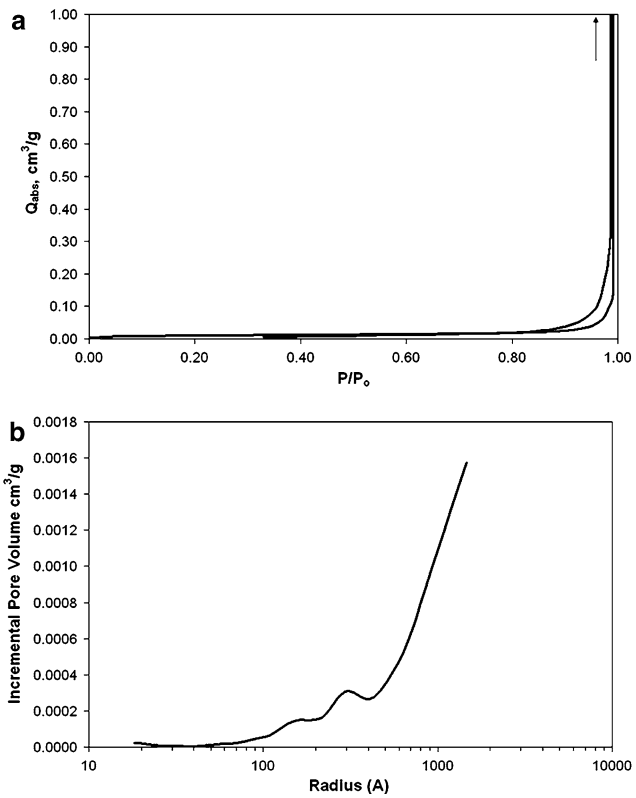

Fig. 2 N_2 sorption isotherms (**a**) and BJH pore size distribution (**b**) of Santa Pudia's limestone (calcarenite)

Table 1 Hydric characteristics of Santa Pudia's limestone (from Rodriguez-Navarro 1994)

	$W(t)_{max}$ (%)	$W(t)_{abs}$ (%)	I_m (%)	V_{abs} (%/h$^{1/2}$)	V_{des} (%/h$^{1/2}$)	V_{cap}, (cm/h$^{1/2}$)	$C_{suc,}$ (g/cm^2 h$^{1/2}$)
Limestone	19.14	14.70	23.17	6.39	3.71	12.9	2.75

$W(t)_{max}$ maximum water content (saturation), $W(t)_{abs}$ maximum water content (absorption), I_m microporosity index, V_{abs} absorption velocity, V_{des} desorption velocity, V_{cap} capillary suction velocity, C_{succ} capillary suction coefficient

damaged stone). Note that mirabilite dehydration and formation of porous aggregates of thenardite upon oven-drying of the salt-laden stone sample may explain the formation of the smaller pores shown in Fig. 1a.

In thin sections, Na-sulfates are recognized as dark microcrystalline aggregates with variable density (Fig. 4). They form complete or partial infillings of pores along the sides of the samples, extending up to 3 mm below the surface. Aggregates of this type are unlikely to have caused salt damage by exerting pressure during crystallization. However, they could be non-pseudomorphic dehydration products of a mirabilite precursor with a different texture (i.e., larger crystals filling the pores), able to exert pressure against the pore walls. Note that some infillings show cracks parallel to the surface, indicative of a decrease in volume at some stage. The variable low density and small crystal size of the Na-sulfate aggregates, together with the heterogeneity of the calcarenite substrate, makes it difficult to document their distribution by X-ray CT analysis.

These observations are consistent with synchrotron radiation energy-dispersive X-ray diffraction analysis of Na-sulfate crystals precipitated within porous oolitic limestone. Such analysis shows that Na-sulfate typically concentrate in a narrow zone underneath the stone skin, approximately 2.6 mm in length, thus resulting in stone damage by means of surface layers scaling (Ioannou et al. 2005). Very little salt (ca. 1% by vol. of thenardite) is detected in such case. La Iglesia et al. (1997) and Rodriguez-Navarro and Doehne (1999a) report similar sodium sulfate-induced weathering pattern in concrete, dolostone and oolitic limestone. It thus appears that Na-sulfate crystallization (and damage) concentrates a few millimeters underneath the stone skin regardless of substrate type. Nonetheless, it is not clear (yet) which phase (mirabilite or thenardite) is responsible for the damage.

Environmental scanning microscopy observation of salt crystals developed in stone slabs show porous aggregates of submicrometer sized thenardite crystals filling large pores (Fig. 5a). Thenardite was identified because it suffered no further dehydration upon ESEM observation at low pressure. Although the typical sponge-like porous structure retaining mirabilite bulk shape (Rodriguez-Navarro and Doehne 1999b) was not observed, it is presumed that the thenardite aggregates formed after mirabilite dehydration. Note, however, that heterogeneous nucleation of Na_2SO_4 over calcite minerals in a limestone pore may induce thenardite

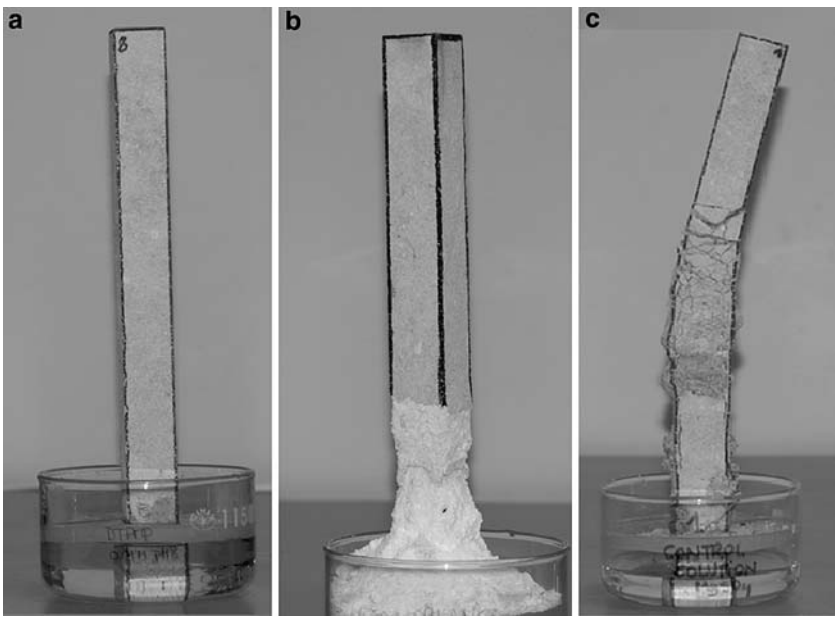

Fig. 3 Sulfate damage in limestone slabs: **a** before crystallization tests; **b** after sodium sulfate crystallization and **c** after magnesium sulfate crystallization

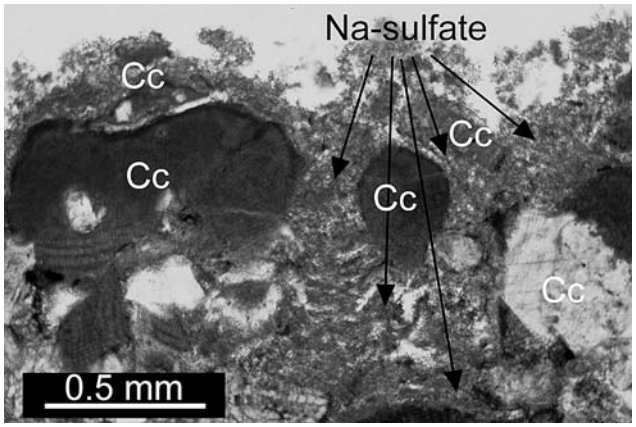

Fig. 4 Optical microscopy photomicrograph of sodium sulfate crystal aggregates (dark masses: Na-sulfate) within calcarenite (Cc: calcite crystals and microfossils) subjected to macroscale salt crystallization test

precipitation and growth at temperatures below 32.4°C (Rodriguez-Navarro et al. 2000a). Thus, the eventual crystallization of thenardite directly from solution is not ruled out.

Macroscale salt crystallization tests: magnesium sulfate

Mg-sulfate shows a decay mechanism based on crack propagation (Fig. 3c). Crystallization of Mg-sulfate significantly reduces the stone porosity (24.2%), but not the mean pore radius (6.4 μm). In contrast to Na-sulfate-laden stone, oven-drying does not seem to induce the formation of small pores in this case (Fig. 1b). The slow thermal dehydration of epsomite (Paulik et al. 1981) may explain this result. Epsomite precipitates deep inside the limestone, filling large and small pores (Fig. 1b), with crystals displaying two distinctive morphologies (Fig. 5b): (a) wax-like aggregates covering calcite grains and filling the smallest pores, and (b) large euhedral bulky crystals present on the sample fracture-surface. A similar crystallization pattern was observed by Rodriguez-Navarro and Doehne (1999a) in the case of halite formed within porous oolitic limestone. While the wax-like aggregates show non-equilibrium morphologies typical of crystals formed at a very high supersaturation, the polyhedral bulky crystals are formed at a lower supersaturation (Sunagawa 1981). These two distinctive morphologies suggest that at least two precipitation events have occurred.

Optical microscopy observations (Fig. 6) reveal that Mg-sulfates are concentrated in bands below the sample surface (1.5 mm thick, top around 2.5 mm below surface). They are composed of elongated crystals oriented perpendicular to the sides of the band, which is a

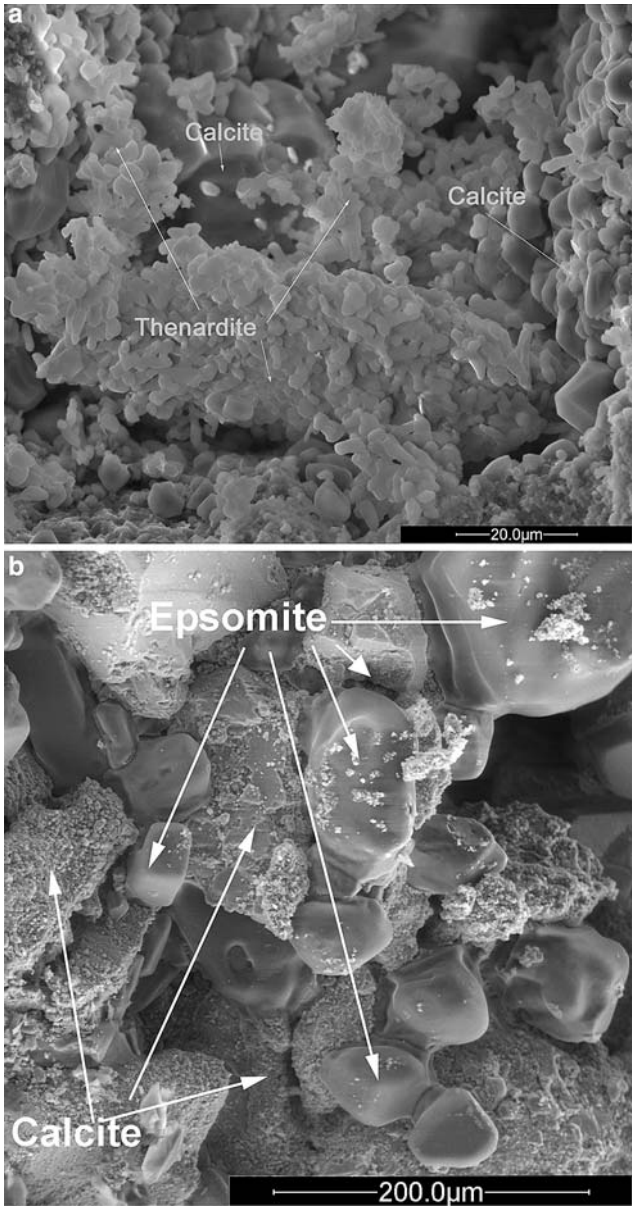

Fig. 5 ESEM micrographs of sulfates grown in calcarenite slab pores (macroscale experiments): **a** sodium sulfate and **b** magnesium sulfate

texture that is compatible with widening of cracks by crystal growth. On the basis of morphological and optical characteristics, the Mg-sulfates are identified as hexahydrite pseudomorphs after euhedral/subhedral epsomite crystals. Hexahydrite of a similar type occurs in pores above the main band (mainly 0–1 mm below the surface) and locally up to 3 mm below that band, both as elongated crystals with a random orientation and as xenotopic intergrowths. In X-ray CT images, massive coarse-grained Mg-sulfate occurrences are easily recognized as nearly parallel bands with some enclosed fragments of the calcarenite substrate (Fig. 7).

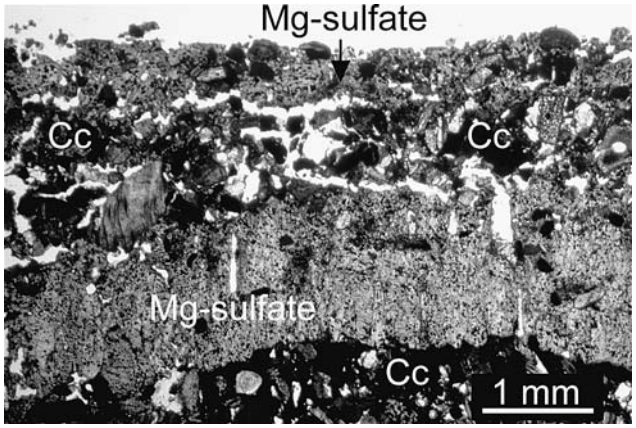

Fig. 6 Optical microscopy photomicrograph of magnesium sulfate crystal aggregates (Mg-sulfate) within calcarenite (Cc: calcite crystals and microfossils) subjected to macroscale salt crystallization test

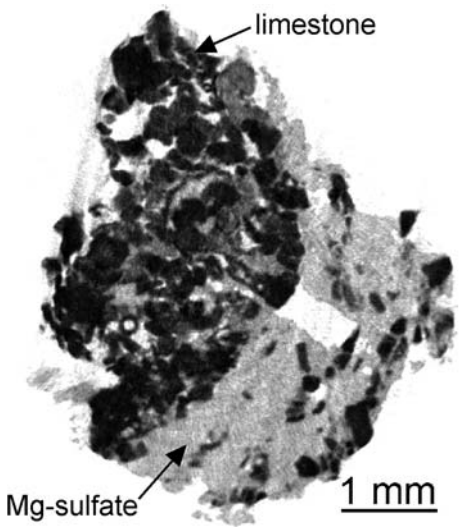

Fig. 7 X-ray CT image of magnesium sulfate crystals (Mg-sulfate) within limestone (calcarenite) slab (equatorial section of the stone block) subjected to macroscale crystallization test

Such Mg-sulfate bands are distributed throughout the whole specimen. ESEM, optical microscopy and X-ray CT observations suggest that Mg-sulfate damage occurred following the initial precipitation of wax-like crystal aggregates formed at a high supersaturation. Cracks developed during this first precipitation event. Subsequently, a new crystallization event led to the formation of larger crystals at a lower supersaturation that deposited in wide bands on the rims of the already formed cracks. The latter appears to have led to the crack-widening process observed macroscopically on the stone block surface (Fig. 3).

In summary, while Na-sulfate typically results in localized damage associated with thin scales, and little salt deposition within the stone pores (although no significant efflorescence is detected), Mg-sulfate causes significant fracturing, generally parallel, but also normal, to the stone surface. The latter salt forms a ''cement'' which infills the stone pores, and somehow prevents the collapse of the cracked slab. It is, however, unclear which phase is responsible for the observed damage in the case of Na-sulfate. Neither is fully clear how Mg-sulfate results in the observed damage, since it appears that most thenardite/hexahydrite crystals filling stone cracks were deposited or grew after the cracks were formed. The microscale ESEM tests helped answering these questions (see below).

Microscale crystallization tests: ESEM dynamic experiments

Figure 8 shows a sequence ESEM photomicrographs of the dynamic study of Na-sulfate deliquescence, followed by mirabilite crystallization and dehydration. Crystallization and growth of mirabilite within the stone pores occurred following a pressure reduction to 6.1 Torr. Damage to the stone due to crystallization pressure buildup was observed at this stage (Fig. 9). Upon reduction of the pressure down to 2.8 Torr, dehydration of mirabilite took place, and thenardite was formed (Fig. 8c). Note that euhedral mirabilite crystals tend to form within the larger pores and dehydrate afterwards. First, this shows that calcarenite damage results from mirabilite crystallization

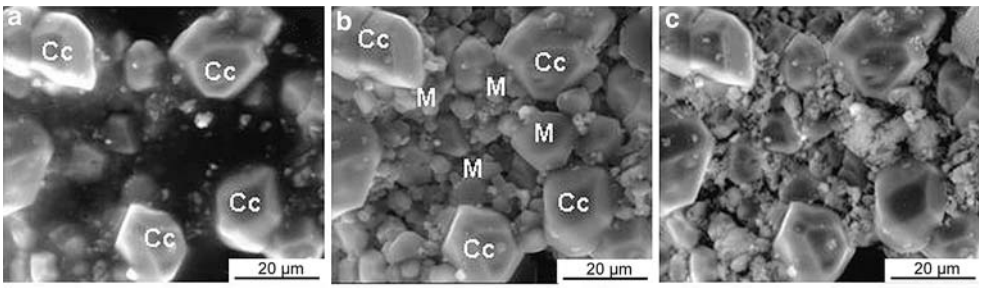

Fig. 8 ESEM microscale crystallization test: sequence of mirabilite crystallization within calcarenite pores: **a** saline solution filling calcarenite pores; **b** mirabilite crystals and **c** thenardite (from mirabilite dehydration). *Cc* calcite; *M* mirabilite

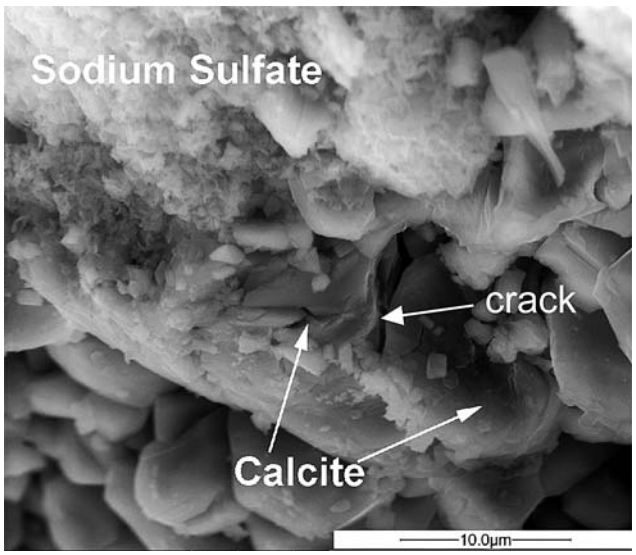

Fig. 9 Detail of calcite grains in sodium sulfate-laden limestone fragment showing granular disintegration/cracks (ESEM in situ microscale experiments)

at relatively low supersaturation (i.e., forming euhedral mirabilite crystals). Second, the growth within the larger pores is consistent with MIP results and the model proposed by Wellman and Wilson (1965).

Massive growth of Mg-sulfate (epsomite) was observed when the ESEM chamber water vapor pressure was reduced to 6.5 Torr (Fig. 10). Formation of a wax-like salt aggregate blanketing the calcite grains and filling (unlike Na-sulfate) both the smaller and larger pores of the limestone substrate was observed. This salt aggregate seems to be formed by sub-micrometer Mg-sulfate crystals. Such morphology is similar to one of the two observed in the macroscale experiments (Fig. 5b), which was suggested to develop during a first crystallization event. However, we observed no bulky euhedral Mg-sulfate crystals. Formation of such crystals is prevented here because only one crystallization event took place in the ESEM chamber. It is suggested that further (fresh) solution supply could result in the (partial) dissolution of the wax-like precipitates, and the formation of larger euhedral crystals that were observed filling the stone cracks in the macroscale tests. Such crystallization behavior is fully consistent with the successive imbibition-drying cycles suggested by Coussy (2006). This author postulates that damage to porous stone due to salt crystallization is an accumulative process resulting from imbibition-drying cycles. Once evaporation has resulted in sufficient supersaturation for a salt to crystallize, further supply of saline solution (undersaturated) will lead to the salt crystals dissolution. The resulting solution will undergo evaporation and supersaturation, followed by a second crystallization event. At a given cycle, damage occurs; however, further crystal growth can take place once damage has occurred. This explains why large Mg-crystals fill the cracks in the weathered calcarenite slabs (macroscale tests).

The crystallization behavior of Mg-sulfate seems to be connected with its ability to sustain a high supersaturation. As the solution evaporates, it retracts towards the smallest pores where capillary suction is highest (Rodriguez-Navarro and Doehne 1999a). In such small pores a high supersaturation can be sustained due to the Laplace effect of curvature (Rodriguez-Navarro et al. 2000b). Crystallization of this salt thus occurs at a very high supersaturation as shown by the observed far-from-equilibrium crystal morphologies (Sunagawa 1981) and the high nucleation density (i.e., very small crystals) (Mullin 1993). All in all, a high crystallization pressure is developed according to the Correns' model (Correns 1949), leading to deep cracking of the stone and the observed damage (Fig. 3).

Role of solution properties on differential damage behavior of sulfates

Our results (Mg-sulfate crystallization) appear to disagree with the generally accepted Wellman and Wilson (1965) theory for salt crystallization. According to this theory, the crystal/saturated solution surface free energy is higher in smaller pores than in coarser ones because of volume constraints. Thus salt crystallization

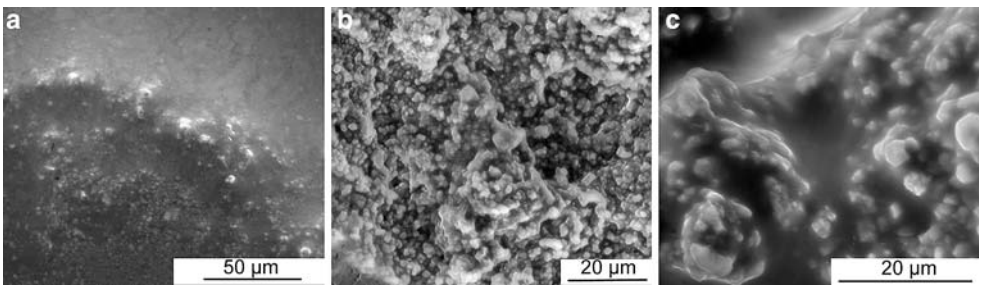

Fig. 10 Magnesium sulfate-laden limestone fragment (ESEM in situ experiments): **a** during evaporation/crystallization; **b** after epsomite crystallization; **c** detail of (**b**) showing anhedral epsomite aggregates filling small and big pores

is thermodynamically not favorable in small pores. This is not what we have observed in the case of Mg-sulfate crystallization. However, it has to be taken into account that ionic transport in porous materials is a competition between salt advection to the evaporation front, and ion diffusion (Pel et al. 2002). Drying rate is the key parameter that controls the prevalence of one mechanism or the other. If the drying is slow, diffusion controls the process (Rijniers 2004). As water evaporates in large pores, ions are transported to small pores where the concentration is initially lower. Finally, crystallization takes place in both large and small pores at a very high supersaturation, thus leading to important damage. This produces the damage pattern observed in the case of Mg-sulfate. If the drying is very fast, salt is transported by advection to the position where evaporation takes place and salts precipitate, that is to say, in large pores. This behavior seems to predominate in the case of the sodium sulfate crystallization tests reported here. Nonetheless, the possibility that Na-sulfate crystallization occurs in all pores (large and small), causing transient stress in the small pores (resulting in cracks) followed by transfer of salt to the larger ones, cannot be ruled out.

Ultimately, the physical properties of a saline solution (i.e., viscosity, density, surface tension and vapor pressure) will control the dynamics of solution flow and evaporation within the porous network of the stone (since environmental conditions, as well as stone support—e.g., permeability—, were kept constant in our tests), and therefore the dynamics of precipitation and salt growth and the resulting damage to the porous substrate. Flow is governed by Poseuille's law, where the driving force is capillary pressure (Lewin 1981). The differential flow behavior of the two saline solutions is mainly due to the differences in viscosity (Table 2). Owing to its higher viscosity, capillary flow is slower in the case of saturated Mg-sulfate solution (compared with that of saturated Na-sulfate solution at the RH and T of the experiment). As a consequence, evaporation occurs faster than the replenishment of the solution by capillary migration from the inside of the stone, and precipitation takes place under the stone surface. The drying-out of solution within a pore opening at the surface occurs by diffusion of water vapor through a layer of the porous solid, and is governed by Fick's law. Once the solution reaches the evaporation front it would be expected that the evaporation rate will be faster in the case of magnesium sulfate, as its vapor pressure is higher (the evaporation rate increases with vapor pressure). However, due to the fact that the evaporation front is placed deeper in the stone (compared with sodium sulfate) the rate of water vapor diffusion and, finally, the effective evaporation rate, would be much lower (Fig. 11). Ultimately, surface scale formation will dominate Na-sulfate crystallization damage, while deep cracking will occur upon Mg-sulfate crystallization. Figure 12 schematically summarizes the differential damage behavior of both salts.

Conclusions

Both sodium and magnesium sulfate are extremely damaging salts, as has been observed in field and laboratory tests. While the mechanism of salt weathering by Na-sulfate consists in detaching of successive stone layers, Mg-sulfate induces crack formation and propagation within the bulk stone. Differences in damage created by Na-sulfate and Mg-sulfate are mainly due to differences in their crystallization pattern since we kept constant the environment variables (RH and T) and the porous support (Santa Pudia's calcarenite). The physical properties of the salt solution, i.e. density,

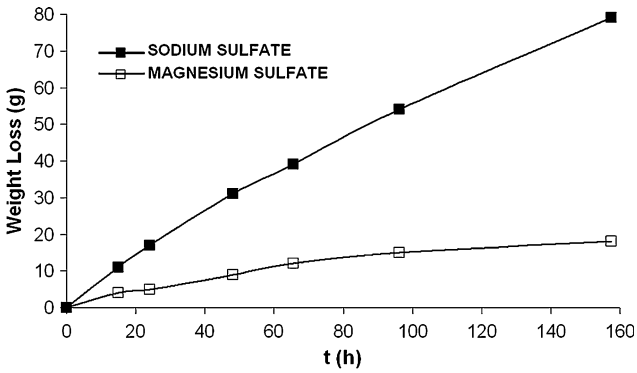

Fig. 11 Evaporation versus time curves for saline solutions in limestone slabs (macroscale crystallization tests)

Table 2 Physical and chemical properties of salt solutions used in crystallization experiments (20°C)

Saturated solution	Concentration (g anhyd./100 ml solution)	Density (g/cm^3)	Surface tension (mN/m)	Viscosity (cP)	Vapor pressure (kPa)
Na_2SO_4	19.4	1.15	75.45	1.834	2.175
$MgSO_4$	33.5	1.29	77.35	7.270	2.781

Data from CRC Handbook of Chemistry and Physics (2005)

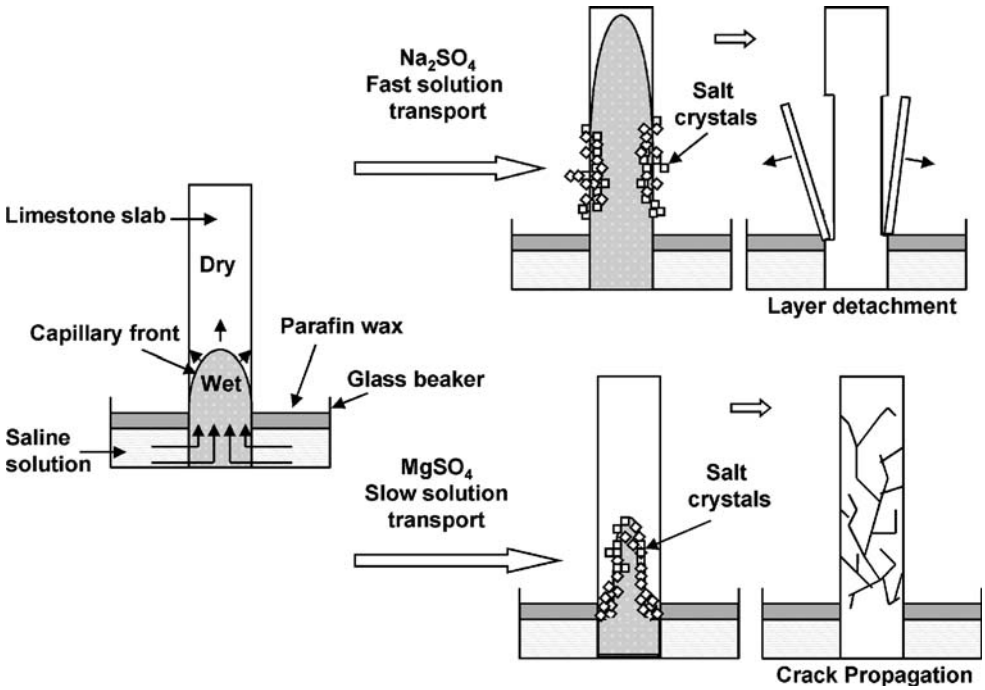

Fig. 12 Schematic comparison of salt damage mechanisms associated with sodium sulfate and magnesium sulfate crystallization in porous limestone

surface tension, and, in particular, viscosity, have a critical effect on the dynamics of solution flow and evaporation within the stone, and therefore, on where crystallization occurs and in what kind of pores, as well as on the resulting damage to porous host materials. High flow rates lead to crystallization inside the stone (but close to the surface) in coarse pores. As a result of low flow rates within the porous network, crystallization takes place inside the stone in both small and big pores. Crystallization taking place on stone surface as efflorescence would avoid/minimize stone damage due to salt crystallization. This can be achieved by acting not only on the crystallization process, i.e., increasing induction times by the addition of crystallization inhibitors (Rodriguez-Navarro et al. 2002; Ruiz-Agudo et al. 2006), but also in the solution transport process within the stone (i.e., high flow rates), as they both play a crucial role in salt damage. The use of compound, such as surfactants, which influence salt crystallization pattern by modifying transport/flow properties of saline solutions inside porous materials (Rodriguez-Navarro et al. 2000b), may reduce salt damage in such building materials. This proposed treatment could enhance the effect of other methods that act mainly modifying the crystallization process (i.e., crystallization inhibitors).

Finally, it is concluded that the combined use of macroscale and in situ microscale salt crystallization tests is highly effective in identifying critical parameters controlling the differential damage behavior of salts. The combined use of in situ as well as conventional techniques to evaluate where and how salts crystallize within porous materials is critical to properly interpret salt weathering mechanisms. This is a crucial step towards the design of new, effective conservation treatment for salt-affected materials.

Acknowledgments This work has been financially supported by the European Commission VIth Framework Program, under Contract no. SSP1-CT-2003-501571, and the research group NRM-179 (Junta de Andalucía, Spain). The ESEM used is from CEAMA (Junta de Andalucía-Universidad de Granada). We thank I. Sanchez-Almazo (CEAMA) for her assistance during the ESEM study. The insightful comments and suggestions of three anonymous referees are acknowledged.

References

ASTM C 88–90 (1997) Standard test method for soundness of aggregate by use of sodium sulfate or magnesium sulfate. Annual Book of ASTM Standard 4.2:37–42

Benavente D, García del Cura MA, Fort R, Ordóñez S (1999) Thermodynamic modelling of changes induced by salt pressure crystallisation in porous media of stone. J Cryst Growth 204:168–178

Benavente D, García del Cura MA, García-Guinea J, Sánchez-Moral S, Ordóñez S (2004) Role of pore structure in salt crystallization in unsaturated porous stone. J Cryst Growth 260:532–544

Braitsch O (1971) Salt deposits: their origin and composition. Springer, Berlin Heidelberg New York

Correns CW (1949) Growth and dissolution of crystals under linear pressure. Discuss Faraday Soc 5:267–271

Coussy O (2006) Deformation and stress from in-pore drying-induced crystallization of salt. J Mech Phys Solids 54:1517–1547

CRC Handbook of Chemistry and Physics (2005) Lide DR (eds), CRC Press, Boca Raton

Dei LM, Mauro M, Baglioni P, Del Fa CM, Fratini F (1999) Growth of crystal phases in porous media. Langmuir 15:8915–8922

De Thury H (1828) Sur la procédé proposé par M. Brard pour reconnaítre immédiatement que ne peuvent pas résister à la gelée, et que l'on désigne ordinairement par les noms de pierres gelives ou pierres gelisses. Annales de Chimie et de Physique 38:160–192

Evans IS (1970) Salt crystallization and rock weathering: A review. Revue Géomorphologie Dynamique 19:153–177

Everett DM (1961) The thermodynamics of frost damage to porous solids. Trans Faraday Soc 57:2205–2211

Flatt RJ (2002) Salt damage in porous materials: how high supersaturations are generated. J Cryst Growth 242:435–454

Good RJ, Mikhail RS (1981) The contact angle in mercury intrusion porosimetry. Powder Technol 29:53–62

Goudie AS (1986) Laboratory simulation of ''the wick effect'' in salt weathering of rock. Earth Surf Processes Landf 11:275–285

Goudie AS (1993) Salt weathering simulation using a single-immersion technique. Earth Surf Processes Landf 18:369–376

Goudie AS, Cooke RU (1984) Salt efflorescences and saline lakes: a distributional analysis. Geoforum 15:563–582

Goudie AS, Viles HA (1997) Salt weathering hazard. Wiley, London

Goudie AS, Viles HA, Parker AG (1997) Monitoring of rapid salt weathering in the central Namib Desert using limestone blocks. J Arid Environ 37:581–598

Gregg SJ, Sing KSW (1982) Adsorption, surface area and porosity. Academic, London

Ioannou I, Hall C, Hoff WD, Pugsley VA, Jacques SDM (2005) Synchrotron radiation energy-dispersive X-ray analysis of salt distribution in Lépine limestone. Analyst 130:1006–1008

Kaneuji M, Winslow DN, Dolch WL (1980) The relationship between aggregate's pore size distribution and its freeze thaw durability in concrete. Cem Concr Res 10:433–441

Katz AJ, Thompson AH (1987) Prediction of rock electrical conductivity from mercury injection measurements. J Geophys Res 92:599–607

La Iglesia A, González V, López-Acevedo V, Viedma C (1997) Salt crystallization in porous construction materials. I. Estimation of crystallization pressure. J Cryst Growth 177:111–118

Levy HA, Lisensky GC (1978) Crystal-structures of sodium-sulfate decahydrate (Glauber's salt) and sodium tetraborate decahydrate (borax): redetermination by neutron-diffraction. Acta Crystallographica B 34:3502–3510

Lewin SZ (1981) The mechanism of masonry decay through crystallization. In: Barkin SM (ed) Conservation of historic stone buildings and monuments. National Academy of Sciences, Washington, pp 120–144

Lowell S, Shields JE (1983) Hysteresis in mercury porosimetry. In: Rossington DR, Condrate RA, Snyder RL (eds) Advances in materials characterization. Plenum Press, New York, pp 133–146

Malin MC (1974) Salt weathering on Mars. J Geophys Res 79:3888–3894

Moscou L, Lub S (1981) Practical use of mercury porosimetry in the study of porous solids. Powder Technol 29:45–52

Mullin JW (1993) Crystallization. Butterworth-Heinemann, Oxford

Naruse H, Tanaka K, Morikawa H, Marumo F (1987) Structure of Na_2SO_4 (I) at 693 K. Acta Crystallographica B 43:143–146

Paulik J, Paulik F, Arnold M (1981) Dehydration of magnesium sulphate heptahydrate investigated by quasi isothermal-quasi isobaric TG. Thermochimica Acta 50:105–110

Pel L, Huinink HP, Kopinga K (2002) Ion transport and crystallization in inorganic building materials as studied by nuclear magnetic resonance. Appl Phys Lett 81:2893–2895

Ramalingom S, Podder J, Narayana Kalkura S, Bocelli G (2003) Habit modification of epsomite in the presence of urea. J Cryst Growth 247:523–529

Rijniers LA (2004) Salt crystallization in porous materials. PhD, Techniche Universiteit Eindhoven, Holland

Rijniers LA, Huinink HP, Pel L, Kopinga K (2005) Experimental evidence of crystallization pressure inside porous media. Phys Rev Lett 94:75503

Robson HL (1927) The system MgSO4–H2O from 68 to 240°. J Am Chem Soc 49:2772–2783

Rodriguez-Navarro C (1994) Causas y mecanismos de alteración de los materiales calcáreos de las catedrales de Granada y Jaén (Causes and mechanisms of decay of the calcareous stones in the Granada and Jaen Cathedrals) (in Spanish). PhD, University of Granada, Spain

Rodriguez-Navarro C (1998). Evidence of honeycomb weathering on Mars. Geophys Res Lett 25:3249–3252

Rodriguez-Navarro C, Doehne E (1999a) Salt weathering: influence of evaporation rate, supersaturation and crystallization pattern. Earth Surf Processes Landf 24:191–209

Rodriguez-Navarro C, Doehne E (1999b) Time-lapse video and ESEM: integrated tools for understanding processes in situ. Am Lab 31:28–35

Rodriguez-Navarro C, Doehne E, Sebastian E (2000a) How does sodium sulfate crystallize? Implications for the decay and testing of building materials. Cem Concr Res 30:1527–1534

Rodriguez-Navarro C, Doehne E, Sebastian E (2000b) Influencing crystallization damage in porous materials through the use of surfactants: experimental results using sodium dodecyl sulfate and cetyldimethylbenzylammonium chloride. Langmuir 16:947–954

Rodriguez-Navarro C, Linares-Fernandez L, Doehne E, Sebastian-Pardo E (2002) Effects of ferrocyanide ions on NaCl crystallization in porous stone. J Cryst Growth 243:503–516

Ruiz-Agudo E, Rodriguez-Navarro C, Sebastian E. (2006) Sodium sulfate crystallization in the presence of phosphonates: Implications in ornamental stone conservation. Cryst Growth Des 6: 1575–1583

Schaffer RJ (1932) The weathering of natural building stones. DSIR, Building Research Special Report No. 18. Stationary Office, London

Scherer GW (1999) Crystallization in pores. Cem Concr Res 29:1347–1358

Scherer GW (2004) Stress from crystallization of salt. Cem Concr Res 34:1613–1624

Steiger M (2005a) Crystal growth in porous materials-I: The crystallization pressure of large crystals. J Cryst Growth 282:455–469

Steiger M (2005b) Crystal growth in porous materials. II: Influence of crystal size on the crystallization pressure. J Cryst Growth 282:470–481

Sunagawa I (1981) Characteristics of crystal growth in nature as seen from the morphology of mineral crystals. Bull Miner 104:81–87

Thaulow N, Sahu S (2004) Mechanism of concrete deterioration due to salt crystallization. Mater Charact 53:123–127

Vaniman DT, Bish DL, Chipera SJ, Fialips CI, Carey JW, Feldman WC (2004) Magnesium sulphate salts and the history of water on Mars. Nature 431:663–665

Wellman HW, Wilson AT (1965) Salt weathering, a neglected geological erosive agent in coastal and arid environments. Nature 205:1097–1098

Weyl PK (1959) Pressure solution and the force of crystallization- A phenomenological theory. J Geophys Res 64:2001–2025

Winkler EM (1994) Stone in architecture. Springer, Berlin Heidelberg New York

Winkler EM, Singer PC (1972) Crystallization pressure of salt in stone and concrete. Geol SocAm Bull 83:3509–3513

Xie P, Beaudoin JJ (1992) Mechanism of sulphate expansion I. Thermodynamic principle of crystallization pressure. Cem Concr Res 22:631–640